Stability and Strength of Transition-Metal Tetraborides and Triborides

R. F. Zhang, D. Legut, Z. J. Lin, Y. S. Zhao, H. K. Mao, and S. Veprek

Phys. Rev. Lett. **108**, 255502 — Published 19 June 2012

DOI: 10.1103/PhysRevLett.108.255502

Stability and Strength of Transition Metal Tetra- and Triborides

R. F. Zhang,[1,2] D. Legut,[3,4] Z. J. Lin,[5,6,*] Y. S. Zhao,[5] H. K. Mao,[6] and S. Veprek[2]

[1]*Theoretical division, Los Alamos National Laboratory, Los Alamos, New Mexico 87545, USA*

[2]*Department of Chemistry, Technical University Munich, Lichtenbergstr. 4, D-85747 Garching, Germany*

[3]*Nanotechnology Centre, VSB-Technical University of Ostrava, CZ-708 33 Ostrava, Czech Republic*

[4]*Atomistic Modelling and Design of Materials, University of Leoben, A-8700 Leoben, Austria*

[5]*LANSCE－LC, Los Alamos National Laboratory, Los Alamos, New Mexico 87545, USA*

[6]*Geophysical Laboratory, Carnegie Institution of Washington, NW Washington, DC 20015, USA*

Abstract

Using density functional theory, we show that the long-believed transition-metal tetraborides (TMB_4) of tungsten and molybdenum are in fact triborides (TMB_3). This finding is supported by thermodynamic, mechanical, and phonon instabilities of TMB_4; and it challenges the previously-proposed origin of superhardness of these compounds and the predictability of the generally used hardness model. Theoretical calculations for the newly identified stable TMB_3 structure correctly reproduce their structural and mechanical properties, as well as the experimental x-ray diffraction pattern. However, the relatively low shear moduli and strengths suggest that TMB_3 cannot be intrinsically stronger than c-BN. The origin of the lattice instability of TMB_3 under large shear strain that occurs at atomic level during plastic deformation can be attributed to valence charge depletion between boron and metal atoms, which enables easy sliding of boron layers between the metal ones.

Recent attempts to design new intrinsically superhard materials ($H \geq 40$ GPa) concentrated on the introduction of light elements forming strong bonds (B, C, N, and O) into transition metals (TM) with high elastic moduli [1-5]. The suggested compounds include 5*d* transition metals diborides (e.g., OsB_2 [4] and ReB_2 [5]) and nitrides such as PtN [6], IrN_2 [7] and η-Ta_2N_3 [8,9]. Although some of these materials have high elastic moduli [4,5], the experimentally determined load-invariant hardnesses are typically below 30 GPa. Osmium diboride possesses high zero-pressure elastic moduli but a low hardness due to the presence of Os-Os layers with weak metallic bonds [10]. Rhenium diboride was believed to be intrinsically superhard [5], but its load invariant hardness is also less than 30 GPa because of electronic and structural instabilities of 5*d* electrons under finite shear strain [11]. Rhenium nitrides, recently synthesized by Friedrich *et al.* [12] under high pressure and temperature, have found much interest because of their large bulk modulus of about 400 GPa, which is higher than that of ReB_2 of 334-371 GPa [5,13]. However, our recent first principles study showed that a combination of thermodynamic instability, relatively low shear moduli and strengths, and relatively soft polar Re-N bonds inherently limits their hardness [14]. These findings strongly challenge the general idea to design intrinsically superhard transition metal diborides based only on their high elastic moduli [3-5].

Great effort has been recently devoted to the synthesis of tetraborides of transition metals by introducing more boron atoms to form 3-dimensional boron network with strong covalent bonds [15-17] because of their economically inexpensive constitutes, relatively high hardness as well as the practically feasible synthetic conditions that do not require high pressure. Using the hardness models, Wang *et al.* [15] suggested that the transition metal tetraborides, such as WB_4 and MoB_4, should be intrinsically superhard. Unfortunately, tungsten tetraboride has load-invariant hardness

less than 30 GPa [16], as recently confirmed by Mohammadi *et al.* [17]. These results raise doubts regarding the predictability of that hardness model (see also [18], and the general stability issue will be unveiled below).

The stability of tetraborides was questioned by Zhang *et al*. [19]. Using the structural evolution method, they reported that MoB_4 in WB_4 structure cannot exist because of its high positive formation energy and presence of imaginary phonon frequencies. More recently, similar thermodynamic instability was addressed for tungsten tetraborides by Liang *et al.* [20]. These researchers have shown that while MoB_4 and WB_4 are unstable, MoB_3 and WB_3 with 2-dimensional boron layers sandwiched between the transition metals are stable. These results arise several questions: 1) Are triborides with the 2-dimensional network be mechanically and dynamically stable? 2) Does the simulated X-ray diffraction (XRD) pattern of the TMB_3 reproduce the experimental data? 3) Could the calculated ideal shear resistance of the triborides support their possible superhardness? In this letter, we show that the WB_4 structure albeit its 3-dimensional covalent boron network, cannot exist due to its general thermodynamic, mechanical, and dynamic instabilities. Instead, the triborides should be experimentally accessible because of their thermodynamic, mechanical and dynamic stability, and because of the agreement of the simulated XRD pattern with the experimental one. We further demonstrate for the first time that, in spite of its 2-dimensional covalent boron network, TMB_3 possesses a high strength comparable to ReB_2 and B_6O. However, because the ideal shear strengths for TMB_3 are much lower than those of c-BN, their intrinsic hardness should be also lower, i.e., they cannot be superhard.

First principles calculations were performed using the VASP code [21] with the generalized-gradient approximation proposed by Perdew and Wang for exchange-correlation functional. Details

of stress-strain calculations can be found in Refs. 22 and 23. Dynamical properties of both TMB_4 and TMB_3 were calculated within the harmonic approximation using the direct method based on the forces calculated via Hellmann-Feynman theorem. To confirm our results, we also used a linear response method based on perturbation theory as implemented in the recent version of VASP code. The resulted phonon dispersion and density of states (DOS) were the same as that using the 2x2x2 supercell method. The equilibrium structural parameters for TMB_4 and TMB_3 (TM=W and Mo) (space groups: $P6_3/mmc$) were obtained by full relaxation of both lattice constants and internal atomic coordination. The relaxed atomic positions for TMB_4 yielded four inequivalent crystallographic sites [TM-2*c* (1/3, 2/3, 1/4), TM-2*b* (0, 0, 1/4), B-12*i* (1/3, 0, 0) and B-4*f* (1/3, 2/3, 0.615)]. The relaxed structure for TMB_3 can be regarded as the absence of four boron atoms at B-4*f* (1/3, 2/3, 0.615) from the TMB_4 structures, which are cross-linking the boron hexagonal layer (Figs. 1a and 1b). The optimized lattice constants of the four borides (a=5.36 Å, c=6.47 Å for WB_4, a=5.21 Å, c=6.86 Å for MoB_4, a=5.20 Å, c=6.34 Å for WB_3, a=5.21 Å, c=6.31 Å for MoB_3) are in good agreement with the previous values [17,20] thus confirming the reliability of present calculations. In addition, the calculated lattice constants of WB_3 show a better agreement with the experimentally reported tungsten borides (a=5.16 Å, c=6.33 Å) than those of WB_4 [17]

The bond structures of WB_4 and WB_3 at equilibrium are shown in Figures 1a and 1b. TMB_4 can be regarded as a three-dimensional boron network (intercalated between the transition metals), consisting of planar hexagonal boron rings and out-of-plane vertical B-B dimers, which connect the neighbor hexagonal boron layers. In comparison, WB_3 consist of the hexagonal boron layer intercalated between adjacent metal layers. The major difference between WB_4 and WB_3 is the absence of the cross-linking B-B dimers in the latter. The isosurface map of electron localization

function (ELF) corresponding to 0.0006 electrons/Bohr^3 for WB_4 and WB_3 are also shown in Figs. 1c and 1d, respectively. A higher value of ELF corresponds to higher electron localization. One can see from Fig. 1c, the strong B-B covalent bonds between the B-B dimers in WB_4 indicate significant electron localization there. One might believe that such a three-dimensional cross-linking of the boron layers should stabilize and strengthen the structure. However, as shown below, the tetraborides are thermodynamically and dynamically instable.

To clarify the thermodynamic stability of TMB_4 and TMB_3, we calculated the formation energy with respect to the transition metal and boron (rhombohedral α-phase) based on the reactions $TM+4B=TMB_4$ and $TM+3B=TMB_3$, respectively. The resulting positive formation energies of WB_4 and MoB_4 are 0.41 eV/atom and 0.28 eV/atom, respectively, suggesting that both tetraborides are thermodynamically unstable. On the contrary, the calculated formation energies of WB_3 and MoB_3 of -0.29 eV/atom and -0.31 eV/atom, respectively, are negative, indicating that both triborides are thermodynamically stable. The distinct thermodynamic stability of tetraborides and triborides is in good agreement with previous work [**19,20**]. However, thermodynamic stability of the triborides does not guarantee their stability against transformation into another phase. Therefore, an analysis of elastic and dynamic stabilities is necessary.

To evaluate the mechanical stability of both triborides and tetraborides, we calculated their single-crystal elastic constants using both linear response method and efficient strain-energy method [**22**]. The obtained "unrelaxed" elastic constants of WB_4 (C_{11}=379 GPa, C_{12}=279 GPa, C_{13}=226 GPa, C_{33}=436 GPa and C_{44}=149 GPa) are in good agreement with the previous calculations (C_{11}=389 GPa, C_{12}=280 GPa, C_{13}=224 GPa, C_{33}=437 GPa and C_{44}=151 GPa [**15**]). Interestingly, we found that the tetraboride structure may spontaneously transform to a lower

energy state if an ionic relaxation is allowed along some shear distortion paths, such as $\varepsilon=(0,0,0,0,0,\delta)$ with $\Delta E/V_0=\frac{1}{4}(C_{11}-C_{12})\delta^2$, and $\varepsilon=(0,0,0,0,\delta,0)$ with $\Delta E/V_0=\frac{1}{2}C_{44}\delta^2$. To confirm this instability, we have introduced a small fluctuation of atomic position of boron atoms within basal planes, the structure cannot recover to the original symmetry. Such mechanical instability may be correlated to its large positive formation energy as discussed above and the dynamic instability as will be shown below. In contrast, both triborides are mechanically stable and the elastic constants (ionic relaxation included) are listed in Table I for WB_3 and MoB_3.

Lattice dynamics was investigated for both TMB_4 and TMB_3. The dispersion relations of WB_4 and WB_3 are shown in Figures 1e and 1f as examples. The phonon dispersion relation of WB_4 exhibits imaginary (negative) frequencies in several important directions showing its dynamic instability at T=0 K. Indeed, the slope of the negative acoustic branch along the Γ-A high-symmetry direction in the vicinity of Γ-point corresponds to elastic constants of C_{44}. Similarly, for Γ-M and Γ-K the lower two branches are also negative close to Γ-point corresponding to negative C_{44} and $C_{66}=(C_{11}-C_{12})/2$. In contrast, the WB_3 phase is stable as there are no imaginary modes. The partial phonon DOS of WB_3 and WB_4 (shown in Figs. 1g and 1h) indicate that the lower frequencies of the total DOS are dominated by lattice dynamics of heavy W atoms and higher frequencies by light B atoms. Moreover, there is a gap in phonon frequencies between ca. 6.5 and 10.5 THz in WB_3 that almost entirely separates higher frequencies dominated by vibrations of B and lower frequencies dominated by W atoms. On the other hand, in WB_4, there is an admixture of phonon states due to dynamics of B and W atoms and no gap in the phonon DOS at the lower frequencies, and some of the optical modes of B atoms are separated by a gap above 25 THz. The imaginary frequencies originate from both, the lattice dynamics of W and B atoms.

The electronic DOS were analyzed in order to obtain insights into the electronic origin of the different stabilities of the tetra- and triborides. The calculated electronic DOS of WB_4, WB_3, MoB_4, and MoB_3 are shown in Fig. 2. Both tetraborides show metallic bonding because of finite value of DOS at the Fermi level (E_F) which originate mostly from *d*-electrons of W or Mo and the *p*-electrons of B. In the triborides, however, the DOS around E_F is lower than in tetraborides and it shows a "splitting" into a pseudogap thus underlying their stability. In the tetraborides, the pseudogap appears far below E_F pointing to the electronic origin of their instability. Obviously, the B-B cross-linking dimers in the tetraborides weakens the bonds within the hexagonal boron layers and cause their less dense packing, because the nearest-neighbor B-B layer distances along the *c* axis of 3.168 Å for WB_3 and 3.154 Å for MoB_3 are shorter than those in tetraborides (3.235 Å for WB_4 and 3.429 Å for MoB_4). The Bader charge density analysis [**24**] shown in Fig. 1 further confirms the inhomogeneous charge transfer of the boron atoms at different crystallographic sites. Comparing the ELF of the tetraboride (Fig. 1c) with that of triboride (Fig. 1d) one can understand that the weakening of the hexagonal boron layers in the former is due to a significant valence charge transfer to the cross-linking boron dimers.

In order to confirm the structure of the experimentally reported borides, we compared the simulated X-ray diffraction (XRD) patterns of triborides and tetraborides with the experimental one. Based on the similarity between tri- and tetraborides (the same space group $P6_3/mmc$), the triboride can be regarded as a boron-deficient tetraborides with absence of B-B dimers. Therefore, a similar XRD pattern is expected for both. We calculated the XRD patterns for WB_4 and WB_3 and compared with the experimental one reported in [**17**]. The results are shown in Fig. 3. Obviously, all the simulated diffraction peaks for WB_3 are in excellent agreement with the experimental ones. In the

simulated XRD pattern of WB_4, however, the intensity the (100), (200), (202) and (210) peaks is clearly higher than those shown in experiment (almost invisible). These results demonstrate that the tungsten borides prepared by Gu *et al.* [16] and Mohammadi *et al.* [17] are WB_3 rather than the long-believed WB_4. None of the lower energy structures of possible WB_4 has a better agreement with experimental XRD pattern than WB_3.

The anisotropic ideal strength of the triborides was obtained from the calculated stress-strain relationships, which are shown in Figures 4a and 4b and also summarized in Table I, and compared with those of hard ReB_2 [22], and superhard B_6O [25], c-BN [23] and diamond [25]. The minimum tensile strengths of WB_3 of 43.3 GPa and MoB_3 of 37.7 GPa are slightly lower than those of ReB_2 and B_6O, but the minimum shear strength along the weakest $(0001)<10\bar{1}0>$ slip system are comparable to those of ReB_2 and B_6O. However, the ideal shear strengths of both triborides are lower than those of c-BN (58.3 GPa [23]) showing their lower shear resistance.

The structures of both WB_3 and MoB_3 before and after the shear instability were analyzed to understand their deformation mechanism. Both compounds show similar instability mode. WB_3 is presented as example in Fig. 4 which shows the structure before and after lattice instability under the $(0001)<10\bar{1}0>$ shear deformation of about 20.4%. It can be seen that after the lattice instability, the originally "flat" boron layer become wavy and the valence charge density difference (VCDD) show charge depletion between the boron and metal atoms indicating breaking of the B-TM bonds (see the arrows in Fig. 4d), which result in a sliding of the boron layers between the tungsten ones. This resembles the first shear instability in ReB_2 described in [11]. A more detailed comparison of the shear instabilities upon a larger shear, as described for ReB_2 in [11] is beyond the scope of the present study.

In summary, we carried out first-principles calculations to evaluate the thermodynamic, mechanical, and phonon stabilities of TMB_4, which have been so far believed to be stable, in comparison with the TMB_3. Electronic structure calculations reveal that the instability of tetraborides is associated with the weakening of the hexagonal boron layers due to strong localization of the *p* electron on the B-B dimers which are connecting adjacent boron layers. The stability issue of transition metal tetraborides challenges the widely used "hardness model" (e.g., [15,26,27]), which incorrectly predict them to be potentially superhard. The triborides are stable because such dimers are absent. The relatively low shear moduli and strength of transition metal triborides indicate that they cannot be intrinsically superhard. An analysis of the deformed atomic and electronic structures reveals that the electronic instability is due to valence charge depletion between boron and metal atoms resulting in sliding of the boron layers between the tungsten ones, which limits their achievable strength.

Acknowledgment

RFZ would like to acknowledge support by Los Alamos National Laboratory Director's Postdoctoral Fellowship. D.L. acknowledges support within the framework of the Nanotechnology - the basis for international cooperation project, Reg. No. CZ.1.07/2.3.00/20.0074 and the IT4Innovations Centre of Excellence project, Reg. No. CZ.1.05/1.1.00/02.0070, both supported by Structural Funds of the European Union and state budget of the Czech Republic. This work is supported as part of the EFree, an Energy Frontier Research Center funded by the DOE, Office of Science and Office of Basic Energy Sciences under Award No. DE-SC0001057. We would also like to thank Prof. G. Kresse for valuable advice for the application of VASP, and Prof. Argon for useful guidance and comments.

References

[1] D. M. Teter and R. J. Hemley, Science **271**, 53 (1996).

[2] S. Veprek, J. Vac. Sci. Technol. A **17**, 2401 (1999).

[3] R. B. Kaner, J. J. Gilman, and S. H. Tolbert, Science **308**, 1268 (2005).

[4] R. W. Cumberland, M. B. Weinberger, J. J. Gilman, S. M. Clark, S. H. Tolbert, and R. B. Kaner, J. Am. Chem. Soc. **127** (2005).

[5] H. Y. Chung, M. B. Weinberger, J. B. Levine, A. Kavner, J. M. Yang, S. H. Tolbert, and R. B. Kaner, Science **316,** 436 (2007).

[6] E. Gregoryanz, C. Sanloup, M. Somayazulu, J. Badro, G. Fiquet, H. K. Mao, and R. J. Hemley, Nat. Mater. **3**, 294 (2004).

[7] A. F. Young, C. Sanloup, E. Gregoryanz, S. Scandolo, R. J. Hemley, and H. K. Mao, Phys. Rev. Lett. **96**, 155501 (2006).

[8] A. Zerr, G. Miehe, J. W. Li, D. A. Dzivenko, V. K. Bulatov, H. Höfer, N. Bolfan-Casanova, M. Fialin, G. Brey, T. Watanabe, and M. Yoshimura, Adv. Funct. Mater. **19**, 2282 (2009).

[9] C. Jiang, Z. J. Lin, and Y. S. Zhao, Phys. Rev. Lett. **103**, 185501 (2009).

[10] J. Yang, H. Sun, and C. F. Chen, J. Am. Chem. Soc. **130**, 7200 (2008).

[11] R. F. Zhang, D. Legut, R. Niewa, A. S. Argon, and S. Veprek, Phys. Rev. B **82**, 104104 (2010).

[12] A. Friedrich, B. Winkler, L. Bayarjargal, W. Morgenroth, E. A. Juarez-Arellano, V. Milman, K. Refson, M. Kunz, and K. Chen, Phys. Rev. Lett. **105**, 085504 (2010).

[13] Y. J. Wang, J. Z. Zhang, L. L. Daemen, Z. J. Lin, Y. S. Zhao, and L. P. Wang, Phys. Rev. B **78**, 224106 (2008).

[14] R. F. Zhang, Z. J. Lin, H. K. Mao and Y. S. Zhao, Phys. Rev. B **83**, 060101R (2011).

[15] M. Wang, Y. W. Li, T. Cui, Y. M. Ma, and G. T. Zou, Appl. Phys. Lett. **93**, 101905 (2008).

[16] Q. Gu, G. Krauss, and G. Steurer, Adv. Mater. **20**, 3620 (2008).

[17] R. Mohammadi, A. T. Lech, M. Xie, B. E. Eeaver, M. T. Yeung, S. H. Tolbert, and R. B. Kaner, Proc. Nat. Ac. Sci. **108**, 10958 (2011).

[18] S. Veprek, A. S. Argon and R. F. Zhang, Philos. Mag. **90**, 4101 (2010).

[19] M. G. Zhang, H. Wang, H. B. Wang, T. Cui, and Y. M. Ma J. Phys. Chem. C **114**, 6722 (2010).

[20] Y. C. Liang, X. Yuan, and W. Q. Zhang, Phys. Rev. B **83**, 220102R (2011).

[21] G. Kresse and J. Furthmüller, Comput. Mater. Sci. **6,** 15 (1996).

[22] R. F. Zhang, S. Veprek, and A. S. Argon, Appl. Phys. Lett. **91**, 201914 (2007).

[23] R. F. Zhang, S. Veprek, and A. S. Argon, Phys. Rev. B **77**, 172103 (2008).

[24] R. F.W. Bader, *Atoms in Molecules-A Quantum Theory* (Oxford University Press, Oxford, 1990).

[25] R. F. Zhang, Z. J. Lin, Y. S. Zhao, and S. Veprek, Phys. Rev. B **83**, 092101 (2011).

[26] F. Gao, J. L. He, E. D. Wu, S. M. Liu, D. L. Yu, D. C. Li, S. Y. Zhang, and Y. J. Tian, Phys. Rev. Lett. **91**, 015502 (2003).

[27] A. Simunek and J. Vackar, Phys. Rev. Lett. **96**, 085501 (2006).

TABLE I. Single-crystal elastic constants c_{ij} (in GPa), the Voigt bulk modulus B_V, shear modulus G_V, and ideal strength (minimum tensile strength σ_{min} and shear strength τ_{min}) of WB_3, and MoB_3 calculated by first principles methods. Previous theoretical results for ReB_2 [22], B_6O [25], c-BN [23], and Diamond [25] are included for comparison.

Compound	Reference	c_{11}	c_{33}	c_{12}	c_{13}	c_{44}	B_V	G_V	σ_{min}	τ_{min}
WB_3	This study	639	470	106	169	262	293	245	$\sigma_{<10\bar{1}0>} = 43.3$	$\tau_{(0001)<10\bar{1}0>} = 37.7$
	[20]	656	479			277				
MoB_3	This study	602	427	106	160	241	276	226	$\sigma_{<10\bar{1}0>} = 37.7$	$\tau_{(0001)<10\bar{1}0>} = 34.1$
	[20]	602	420	106	166	247	276	222		
h-ReB_2	[22]	631	1015	158	134	257	348	274	$\sigma_{<\bar{1}2\bar{1}0>} = 58.5$	$\tau_{(0001)<10\bar{1}0>} = 34.4$
h-B_6O	[25]	603	459	109	50	179	231	218	$\sigma_{<10\bar{1}0>} = 53.3$	$\tau_{(0001)<10\bar{1}0>} = 38.0$
c-BN	[23]	786		172		445	376	390	$\sigma_{<111>} = 55.3$	$\tau_{(111)<11\bar{2}>} = 58.3$
Diamond	[25]	1079		124		578	442	528	$\sigma_{<111>} = 82.3$	$\tau_{(111)<11\bar{2}>} = 86.8$

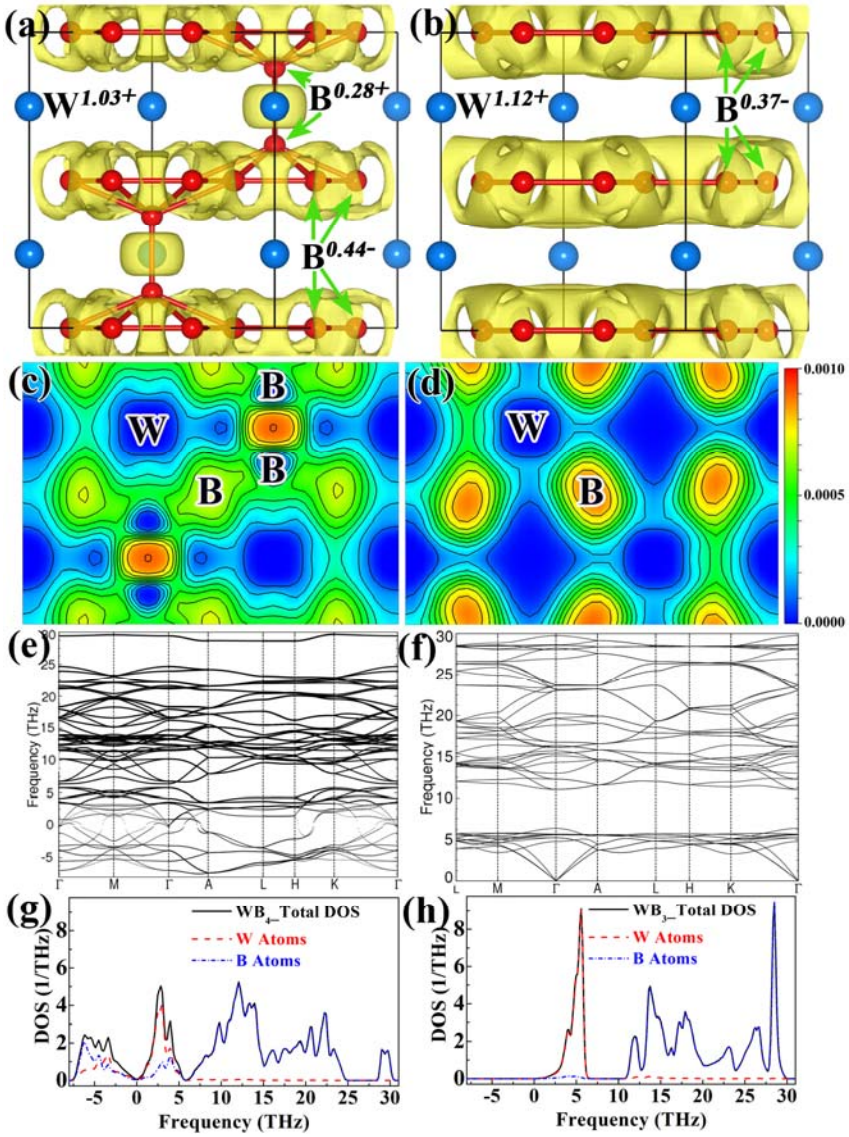

FIG. 1 (color online). Bond structures at equilibrium for (a) WB_4 and (b) WB_3. The isosurfaces maps of the electron localization function (ELF) correspond to 0.0006 electrons/Bohr^3, the large blue and small red spheres represent W and B atoms, respectively. Maps of the electron localization function (ELF) on the $(10\bar{1}0)$ plane for (c) WB_4 and (d) WB_3. Calculated phonon dispersion curves for (e) WB_4 and (f) WB_3. The phonon density of states for (g) WB_4 and (h) WB_3. The numbers close to W and B atoms in Figs. 1a and 1b are the corresponding Bader charges.

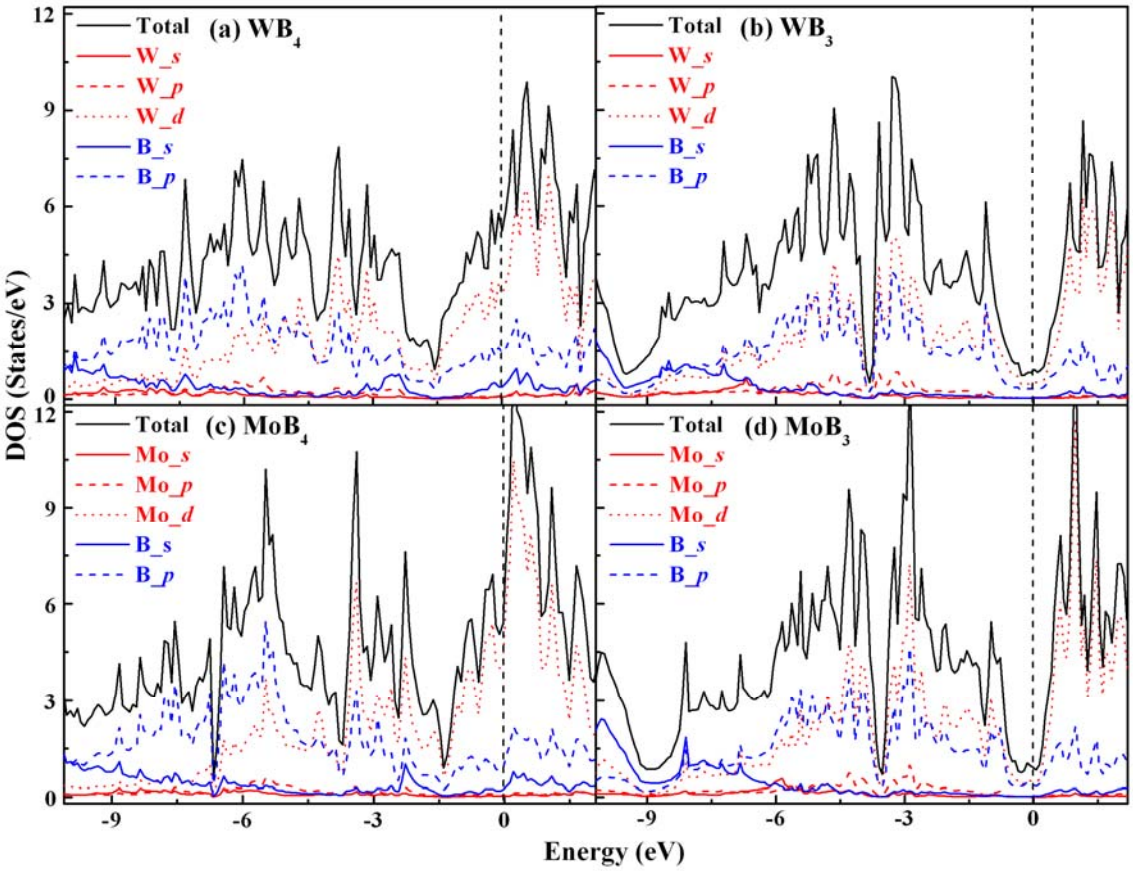

FIG. 2 (Color online). Total and partial electronic density of states of (a) WB_4, (b) WB_3, (c) MoB_4, and (d) MoB_3. The vertical dashed lines indicate the Fermi levels.

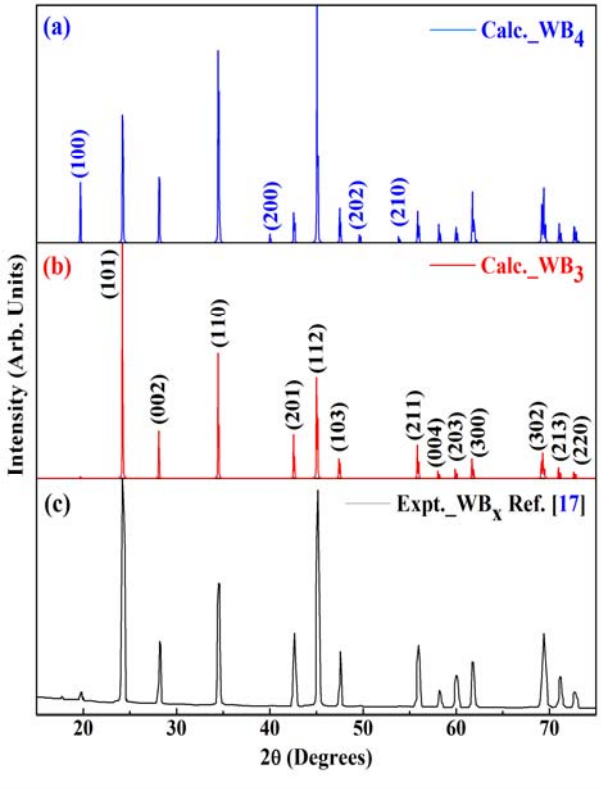

Fig. 3 Simulated XRD curves for (a) WB_4 and (b) WB_3. (c) Experimental XRD pattern for WB_x reproduced from Ref. [17].

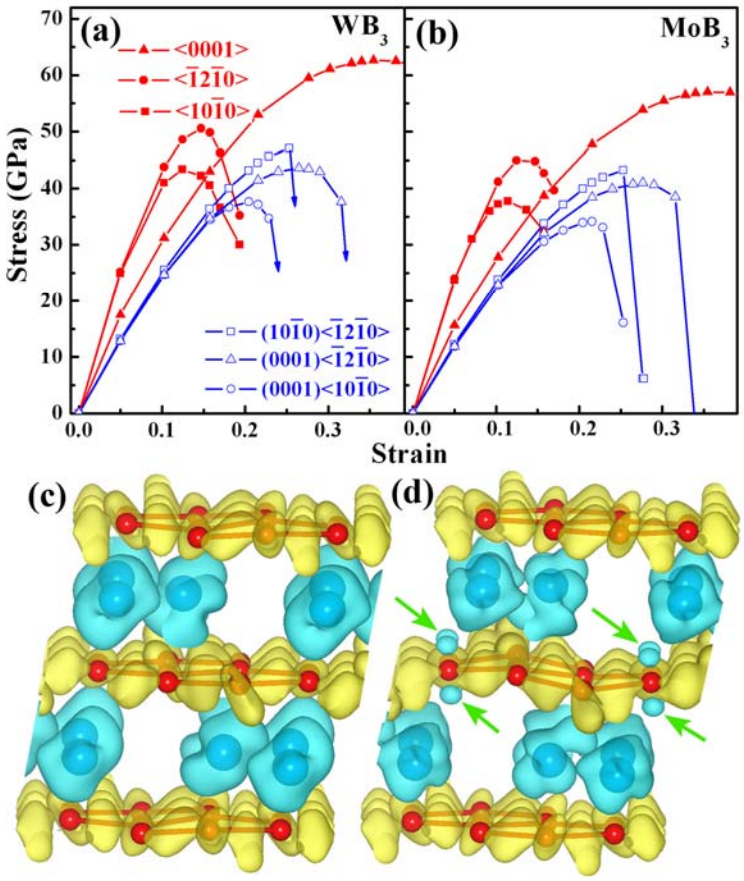

FIG. 4 (Color online). Stress-strain relationships for (a) WB_3 and (b) MoB_3. Curves with solid symbols indicate tension deformations and curves with open symbols denote shear deformations. The isosurfaces of deformed valence charge density difference (VCDD) of WB_3 at shear strain of (c) γ=0.2044 (before) and (d) γ=0.2531 (after lattice instability) in the $(0001)<10\bar{1}0>$ slip system. The isosurfaces of VCDD correspond to of +/-0.016 electrons/Bohr^3, large and small spheres represent tungsten and boron atoms, respectively. The arrows highlight the charge depletion states.